

# X-Ray Observations of $\gamma$ -Ray Burst Afterglows

Filippo Frontera

Physics Department, University of Ferrara, Ferrara, Italy  
and  
Istituto Astrofisica Spaziale e Fisica Cosmica, CNR, Bologna, Italy

**Summary.** The discovery by the *BeppoSAX* satellite of X-ray afterglow emission from the  $\gamma$ -ray burst which occurred on 28 February 1997 produced a revolution in our knowledge of the  $\gamma$ -ray burst phenomenon. Along with the discovery of X-ray afterglows, the optical afterglows of  $\gamma$ -ray bursts were discovered and the distance issue was settled, at least for long  $\gamma$ -ray bursts. The 30 year mystery of the  $\gamma$ -ray burst phenomenon is now on the way to solution. Here I review the observational status of the X-ray afterglow emission, its mean properties (detection rate, continuum spectra, line features, and light curves), and the X-ray constraints on theoretical models of  $\gamma$ -ray bursters and their progenitors. I also discuss the early onset afterglow emission, the remaining questions, and the role of future X-ray afterglow observations.

## 1 Introduction

The investigation into the nature and origin of celestial Gamma-Ray Bursts (GRBs) has been one of the major challenges of high energy astrophysics, since they were discovered by chance about 30 years ago with the *VELA* satellites [77]. The GRB origin remained uncertain even when the *Burst and Transient Source Experiment (BATSE)* experiment aboard the *Compton Gamma-Ray Observatory (CGRO)* in the 1990s provided a much larger sample of GRBs (about 3000 events). Many outstanding results were obtained with BATSE, among them the completely isotropic distribution on the sky of GRBs and the inconsistency of the GRB number versus peak intensity relation with a homogeneous volume distribution in space, implying a deficit of faint bursts [18,96,114]. Two main explanations were given for these statistical properties: either GRBs have their origin in neutron stars distributed in a large Galactic halo at more than 100 kpc distance [17,19,61,83,136,156] or GRBs have an origin in sources at cosmological distances [96,98,99,100,108,115,137,155].

It was recognized (see, e.g., [39]) that the identification of a GRB counterpart at other wavelengths was needed in order to make a breakthrough in setting the distance scale of GRBs. Now the distance scale issue of at least the long ( $> 1$  s) GRBs has been definitely settled thanks to the X-ray astronomy mission *BeppoSAX*, an Italian satellite with Dutch participation[12].

*BeppoSAX* has also provided the most exciting results of the last six years in GRB astronomy. The high performance of *BeppoSAX* for GRB studies is due to a particularly well-matched configuration of its payload, with both Wide Field and Narrow Field Instruments (WFIs and NFIs). The WFIs consist of a  $\gamma$ -ray (40–700 keV) all-sky monitor, the *Gamma-Ray Burst Monitor (GRBM)* [43], and two Wide-Field Cameras (WFCs) instruments covering the 2–28 keV energy band [76]. The NFIs include four focusing X-ray (0.1–10 keV) telescopes (one *Low-Energy Concentrator Spectrometer (LECS)* [120] and three *Medium-Energy Concentrator Spectrometers (MECS)* [13]). The NFIs also have two higher energy direct viewing detectors (the *High Pressure Gas Scintillation Proportional Counter (HPGSPC)* [88] and the *Phoswich Detector System (PDS)* [43]).

The *BeppoSAX* capability of precisely localizing GRBs was soon tested, only one month after first light of the satellite, with the detection of GRB960720 [126]. Starting from December 1996, at the *BeppoSAX* Science Operation Center, an alert procedure for the search of simultaneous *GRBM* and *WFCs* detections of GRB events was implemented. Thanks to this procedure, the first X-ray afterglow of a GRB, GRB970228, was discovered on 28 February 1997 [23]. Simultaneously, an optical counterpart of the X-ray afterglow source was detected [164]. Less than two months later, the first optical redshift ( $z = 0.835$ ) of GRB970508 was obtained thanks to the prompt localization provided by *BeppoSAX*, [102]. The location of GRBs at cosmic distances was definitely established. At the same time, an exciting result on the GRB source properties came from radio observations of the same event: the radio afterglow exhibited rapid variations for about one month due to interstellar scintillations [40]. Thus, only a very compact source, expanding highly relativistically, could be the origin of GRBs [40].

Since the first detection of an X-ray afterglow, many other GRB afterglows have been detected, mainly with *BeppoSAX* and, less often, with other satellites, i.e., the *Röntgensatellit (ROSAT)*, the *Rossi X-ray Time Explorer (RXTE)*, the *Advanced Satellite for Cosmology and Astrophysics (ASCA)*, the *Chandra X-ray Observatory-AXAF (CHANDRA)*, and the *XMM-Newton (XMM)*. In this paper I review the status of our knowledge of GRB X-ray afterglows and discuss their implications. In Sect.2, I discuss the measured afterglow properties (detection rate, continuum spectral properties, light curves and X-ray line features); in Sect. 3, I discuss the early afterglow emission and its distinctive features with respect to the prompt emission; and in Sect4, I summarize the open questions and the prospects for future X-ray afterglow observations.

## 2 X-Ray Afterglow Observations and Properties

Tables 1, 2 and 3 summarize the main results of the X-ray searches for GRB afterglows. In the following provides further elaboration.

## 2.1 X-Ray Afterglow Detection Rate

Table 1 lists the information on GRB follow-up observations of X-ray afterglows as of December 2001. Two X-ray rich events, GRB011030 [51] and GRB011130 [141], were not included in the list. GRB011030 was observed by *Chandra* [66] following the discovery of a radio transient in the GRB error box [162] and an X-ray source was detected but no fading observed [66]. GRB011130 was also observed by *Chandra* and several X-ray sources were detected but no conclusions could be drawn as to their association with the GRB [142]. As can be seen, most of the 43 GRBs listed in Table 1 were promptly localized with the *BeppoSAX* WFCs, with the *RXTE Proportional Counter Array (PCA)*, the *All Sky Monitor (ASM)* and the 3rd *Interplanetary Network (IPN)* contributing some additional examples. The minimum starting time of the follow-up observations ranges from 2–3 hr for *RXTE*, to 5–6 hr for *BeppoSAX*, to longer times for the other satellites. Given its limited sensitivity, the *RXTE PCA* has provided positive results only for very strong afterglow fluxes (few mCrab) and for a limited time interval. Unfortunately most of these PCA events were not followed up with more sensitive instruments.

The criterion for establishing the afterglow nature of an X-ray source is its fading on time scales of a few hours or days. Unfortunately, for the weakest sources this fading could not be well established, as the detected flux was very close to the instrument sensitivity limit. In these cases the source found in the GRB error box could be a serendipitous field source unrelated to an X-ray afterglow, even though the probability of such a chance coincidence is low (see the notes to Table 1). With this caveat in mind, 37 of the followed 43 GRBs (86%), show X-ray afterglows at a level  $> 10^{-13}$  erg cm $^{-2}$  s $^{-1}$  in the 2–10 keV band. Thus, the detection rate of X-ray afterglows is about two times higher than that for optical afterglows (see the chapter by E. Pian). Therein lies the mystery of the so-called "dark bursts", i.e., bursts which show an X-ray afterglow but not optical emission (see Section 4).

## 2.2 X-Ray Afterglow Continuum Spectra

The spectral shape of the X-ray afterglow emission gives important information about establishing the emission mechanisms. An initial question was whether the X-ray continuum emission was thermal or nonthermal. The X-ray afterglow of GRB970228 showed [45] that, in the X-ray range (0.1–10 keV), a blackbody model was not acceptable. The photon spectrum was well fit with a simple photoelectrically absorbed power-law (see Table 2). This spectral shape has been found in all X-ray afterglows known, although for some GRBs (GRB980329 [177] and GRB981226 [47]), in which thermal models were tested, it was found that the data do not have sufficient signal-to-noise to discriminate between power-law and blackbody models.

Table 2 reports the best fit power-law photon indices  $I$  (where the photon index  $I$  is related to the flux density  $F$  spectral index  $\alpha$ ,  $F_\nu \propto \nu^{+\alpha}$ , by

$I = \alpha - 1$ ) and absorbing hydrogen column densities  $n_H$ . The values reported in square brackets were kept fixed during the fit. For comparison, the Galactic hydrogen column densities  $n_H^G$  values along the GRB directions are also reported [32]. The best fit values of  $I$  and  $n_H$  are available for only the brightest of the detected afterglows. Most of the spectra have been determined up to 10 keV, and in only one case (GRB990123) was the source detected up to 60 keV with the *BeppoSAX* PDS instrument, also confirming the power-law shape.

As can be seen from Table 2, due to the low statistical quality of the X-ray data, in many cases the Galactic  $n_H^G$  was assumed (in square brackets) in the spectral fitting. In the cases for which estimates of  $n_H$  were derived, they are consistent, within the uncertainties, with the Galactic values, except for seven GRBs (GRB970828, GRB980329, GRB980703, GRB990510, GRB000926, GRB001109, GRB010222) for which the derived  $n_H$  is significantly higher than the Galactic value. Since the reported  $n_H$  values have been derived assuming only local, Galactic absorption ( $z = 0$ ), the true  $n_H$  may be even higher, if it is in the host galaxy or in the ambient medium around the burst. For example, Weiler et al [170] (see also the chapter by Weiler et al. in [171]) found that significant amount of optical extinction can be ascribed to the burst host galaxy or its local surroundings.

The best fit photon indices  $I$  range from  $\sim -1.5$  to  $\sim -2.8$  with a roughly Gaussian distribution with standard deviation  $\sigma_I \approx 0.4$  and mean value  $\langle I \rangle = -1.95 \pm 0.03$ , which is very close to the power law index of the well known synchrotron source, the Crab Nebula ( $I = -2.1$ ). The only evidence of spectral variability is for GRB970508 and GRB00026 listed in Table 2. For comparison, the prompt 2–700 keV emission from GRBs with detected X-ray afterglow is generally well described [48] by a photoelectrically absorbed, smoothly broken power-law [9] with low-energy index  $\alpha_1$  (below the break), high energy broken index  $\alpha_2$  above the break, and peak energy  $E_p$  of the  $EF(E)$  spectra, all which evolve rapidly with time. One relevant feature of these spectra is that, at the GRB onset,  $E_p$  is generally above the energy passband of the *BeppoSAX* GRBM [48] (see the example in Fig. 1).

Several hints, such as the non thermal shape of the spectra and detection of polarized emission from the optical counterparts of two afterglows (GRB990510 [27,174] and GRB990712 [143]) point to synchrotron radiation as the basic emission mechanism of the electromagnetic radiation from GRB afterglows. Also, in the case of the prompt emission, synchrotron radiation appears to play an important role, even if other emission processes such as Inverse Compton (IC) may contribute at the earliest times (see, e.g., [48]). Synchrotron radiation is expected within the framework of the fireball model (see, e.g., reviews by Piran [124,125] and references therein) as a result of the interaction between a relativistically expanding fireball and the external medium ("external shock"). Detailed calculations of the expected synchrotron spectral shape and its time evolution have been carried out for various external

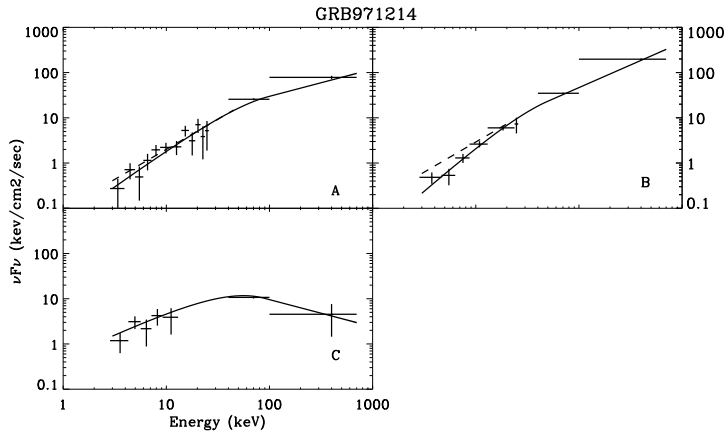


**Fig. 1.** Spectral evolution of GRB971214 in three contiguous time intervals, A (8 s), B (12 s) and C (18 s), in which the GRB light curve was subdivided [48].

medium conditions (homogeneous medium [150], or radially declining density wind [21]). Also the effect of IC scattering of low-energy synchrotron photons on shock-accelerated electrons has been investigated (see, e.g., [118,153]).

Following Sari et al. [150], for the case of a homogeneous medium, the instantaneous synchrotron energy spectrum  $F(E)$  is schematically described by a multi-broken power-law, with four different slopes. At low frequencies, the flux density  $F_\nu \propto \nu^2$  holds up to the synchrotron self-absorption (SSA) frequency  $\nu_{SSA}$ , then  $F_\nu \propto \nu^{1/3}$  from  $\nu_{SSA}$  up to the peak frequency  $\nu_m$  ( $\nu_m$  corresponds to the minimum-energy of the shock-accelerated electrons). At still higher frequencies, the spectrum is related to the energy distribution of the electrons, which is assumed to exhibit a power law shape  $N(E_e) \propto E_e^{-p}$  ( $E_e$  is the electron energy) from  $\nu_m$  up to the cooling frequency  $\nu_c$  ( $\nu_c$  corresponds to the highest energy electrons that cool more rapidly than the expansion time of the source), by means of  $F_\nu \propto \nu^{-(p-1)/2}$ , while above  $\nu_c$ ,  $F_\nu \propto \nu^{-p/2}$ . Depending on the shock evolution, fully adiabatic or fully radiative, the characteristic frequencies  $\nu_m$  and  $\nu_c$  and the maximum flux density  $F_m$  vary in different ways with time. For the fully adiabatic case,  $\nu_m \propto t^{-1/2}$  and  $\nu_c \propto t^{-3/2}$ . For the fully radiative case  $\nu_m \propto t^{-12/7}$  and  $\nu_c \propto t^{-2/7}$ . In the latter case,  $F_m$  also changes with time as  $F_m \propto t^{-3/7}$ . The different time behaviour of the characteristic frequencies is thus expected to affect not only the spectral evolution of the emission but also the time behaviour of the afterglow light curves (see Section 2.3).

The multiwavelength spectrum of the GRB970508 afterglow fits this scheme very nicely [49]. Unfortunately, broad band spectra are available for only a very limited number of GRBs. An attempt to collect the available data to esti-

mate the multiwavelength spectra of GRB afterglows was performed [94], but the data are still scarce. Most of the few available spectra are consistent with the synchrotron shock model (in addition to GRB970508, GRB971216 [30], GRB980703 [168], and GRB991216 [41]). However, in two cases (GRB000926 [64] and GRB010222 [179]), the multiwavelength spectra clearly deviate from the shape expected from the synchrotron model. In both cases, the radio and optical data fit a synchrotron spectrum very well, but the extrapolation of the spectrum to X-rays is below the measured X-ray flux density. Harrison et al. [64] interpret this mismatch as due to the presence of a self-Inverse Compton component. The ambient medium density derived is  $\sim 30 \text{ cm}^{-3}$ , which is higher than the average InterStellar Medium (ISM) density in a typical galaxy ( $\sim 1 \text{ cm}^{-3}$ ), but is consistent with a diffuse interstellar cloud such as those found in star forming regions.

Assuming a synchrotron origin, the photon indices  $I$  listed in Table 2 permit an estimate to be made of the power-law index of the energy distribution of the electrons accelerated in the external shocks. Given that most of the X-ray afterglow measurements were performed considerably after the main event (see Table 1 for the start times), these can be reasonably assumed to be taken in the regime of  $\nu > \nu_m$ , when the peak of the spectrum had moved toward the optical range. Thus, the electron index  $p$  is related to the photon index by one of two equations: either  $p = -2I - 1$  or  $p = -2I - 2$ , depending whether the X-ray band is between  $\nu_m$  and  $\nu_c$  (fast cooling) or beyond these frequencies (slow cooling). From the mean value of  $I$ , we can derive a mean value of the electron index  $\langle p \rangle$  in the range from  $\sim 2$  to  $\sim 3$ , depending on the cooling regime.

### 2.3 Time Behaviour of the X-Ray Afterglow Light Curves

One of the most peculiar properties of the X-ray afterglow light curves is their power-law decay ( $F(t) \propto t^{+\beta}$ ). The power-law fading was already noted in the first X-ray afterglow source 1SAX J0501.7+1146 associated with GRB970228 [23]. The X-ray fading slope ( $\beta_X = -1.33_{-0.13}^{+0.11}$ ) was consistent with that ( $\beta_{opt} = -1.46 \pm 0.16$ ) of the simultaneously discovered optical counterpart [164]. The power-law decay index and the photon index of the GRB970228 afterglow (see values in Table 2) were also found to be consistent with the relationship predicted by the fireball model and gave strong support to that model (see e.g., [173]). Almost all other X-ray afterglow sources discovered so far show a similar power-law decay or, in a few cases, a broken power-law. Table 2 reports the best fit temporal indices,  $\beta$ , measured. Apart from GRB980425, which will be discussed separately below, the power-law indices are distributed like a Gaussian with mean value  $\langle \beta \rangle = -1.30 \pm 0.02$ , and standard deviation  $\sigma_\beta \approx 0.35$ . A relevant feature of the light curves is that their extrapolation back to the time of the GRB event is, in general, consistent with the tail of the prompt X-ray light curve. This fact is in some

cases directly misured (GRB970228 [23] and GRB970508 [127]) and in other cases is inferred from a different approach (see Section 3).

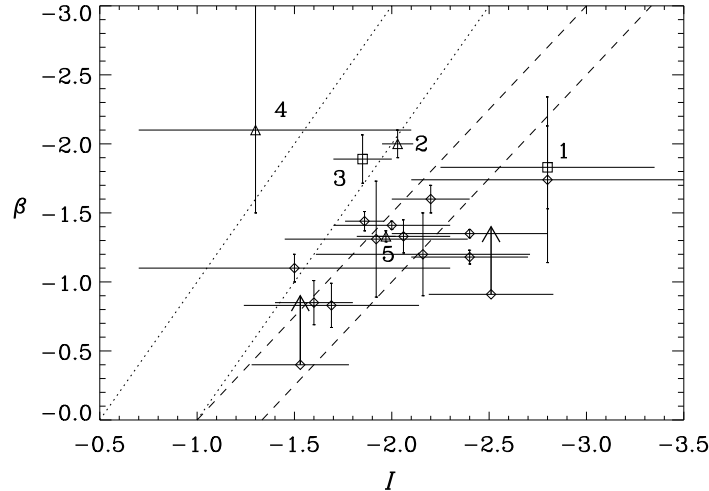


**Fig. 2.** The measured temporal index  $\beta$  vs. the photon index  $I$  of GRB afterglows. The GRBs with evidence of a break in their X-ray light curves are indicated with triangles, while those with high temporal index ( $\beta < -1.8$ ) are indicated with squares. 1: GRB980519, 2: GRB990510, 3: GRB000926, 4: GRB010214, 5: GRB010222. For GRB990510 the temporal index estimated by [122] is quoted. The region between the dashed lines is for a spherical expansion while the region between the dotted lines is for an expanding jet.

In a few cases (GRB990510 [121], GRB010222 [179] and GRB010214 [60]) comparison of the intensity level of the tail of the prompt emission with the late afterglow light curve (start time several hrs after the GRB event), shows that a broken power-law may be more consistent with the data. In Table 2 the power-law indices and break times of these GRBs are reported. The X-ray breaks are found to be consistent with those seen in the optical light curves (see [63,74,158] for GRB990510, and [95] for GRB010222).

The interpretation of achromatic breaks in the light curves of GRB afterglows has been discussed by various authors. In the framework of the fireball model, a break is expected if the relativistically expanding material is concentrated within a cone with angular width  $\theta_c$ . As long as the Lorentz factor  $\Gamma$  of the outflowing material is larger than  $1/\theta_c$ , due to relativistic beaming, the radiation is emitted within an angle  $\theta_b = 1/\Gamma$  from the cone axis, with  $\theta_b < \theta_c$ . When  $\Gamma$  drops below  $1/\theta_c$ , the observer begins to see the edge of the cone and then the effect of the collimated outflow, which causes a light curve steepening. At the same time ( $t_j$ ), the jet begins to expand sideways, increas-

ing the rate of decrease of the emitted radiation even more. This model has been discussed and detailed for various external conditions by several authors (see e.g., [80,117,119,140,151] and references therein).

Assuming synchrotron radiation, adiabatic expansion and a homogeneous ambient medium, following Sari et al. [151], the energy flux density, if  $\nu_m < \nu < \nu_c$ , is given by

$$F_\nu(t) \propto t^{-3(p-1)/4}$$

for  $t \leq t_j$  and

$$F_\nu(t) \propto t^{-p}$$

for  $t \geq t_j$ . However, if  $\nu > \nu_c > \nu_m$ ,

$$F_\nu(t) \propto t^{-3p/4+1/2}$$

for  $t \leq t_j$  and

$$F_\nu(t) \propto t^{-p}$$

for  $t \geq t_j$ . In both cases, after the break the light curve has the same slope. In this framework, the temporal decay index,  $\beta$ , and the photon index,  $I$ , are strictly related: in the case of spherical expansion

$$\beta = 3I/2 + 3/2$$

for  $\nu < \nu_c$  and

$$\beta = 3I/2 + 2$$

for  $\nu > \nu_c$ . In the case of an expanding jet

$$\beta = 2I + 1$$

for  $\nu < \nu_c$  and

$$\beta = 2I + 2$$

for  $\nu > \nu_c$ . The above predictions can be easily tested with the available data.

In Fig. 2, the values of  $(I, \beta)$  for each afterglow source are shown (see also earlier test [159]). Even though the statistical uncertainties do not allow us to draw firm conclusions from this diagram, a clustering of the data within the region expected from a spherical expansion is apparent. The above derived mean values of  $I$  and  $\beta$  confirm this. Indeed, assuming  $I = -1.95$ , in the hypothesis of spherical expansion,  $\beta$  is expected to be in the range from -0.9 to -1.4, depending on whether  $\nu < \nu_c$  or  $\nu > \nu_c$ , while in the case of an expanding jet,  $\beta$  is in the range from -1.9 to -2.9. This result seems to disagree with the results of Frail et al.[42] who, by examining the multiwavelength light curves of a sample of 17 GRB afterglows find a break in a large fraction of them which they interpret as evidence for an expanding jet. They derive the jet opening angle for each of them. Even though both samples are still too small to infer general properties, our result can still be consistent with those of Frail et al. [42]. Only 10 of the 17 GRBs appear in Table 2 and, for



most those 10, either the derived X-ray parameters refer to epochs before the breaks reported by Frail et al. or the X-ray light curves are of poor statistical quality.

As can be seen from Fig. 2, the position of three events is consistent with the jet region between the dotted lines. Two show evidence of a break in their X-ray light curves (GRB010510, GRB010214), and one (GRB000926) exhibits a high temporal index (but it shows a break in the optical light curve [132]). The X-ray light curve of GRB990510 was discussed by Pian et al. [122], who found it consistent with the jet model and derived the following parameters of the jet and circumburst medium: ambient density of  $0.13 \text{ cm}^{-3}$ , electron energy distribution index of  $p = 2$ , isotropic equivalent energy of  $E_0 = 5 \times 10^{53} \text{ erg}$ , and opening angle of  $\theta_c = 2.7^\circ$ .

In the case of GRB010222, which is within the spherical expansion region of Fig. 2 but shows a break consistent with that observed in the optical band [95], in't Zand et al. [179] interpret it as probably due to the transition of a spherically expanding fireball from a relativistic to a non-relativistic phase (NRP) [28]. Also in this case a break is expected when the shock wave has swept up a rest-mass energy equal to its initial energy [87,132,173]. Assuming synchrotron radiation from an adiabatically cooling shock as above, the change in the temporal index is now shallower than for the case of an expanding jet. After the transition to NRP, we have

$$\beta = 3I + 18/5$$

for  $\nu < \nu_c$  and

$$\beta = 3I + 5$$

for  $\nu > \nu_c$ . In the case of the GRB010222, in spite of the fact that the measured values of  $\beta$  and  $I$  after the break are still inconsistent with each other assuming NRP, this model predicts values of the electron index  $p$ , when derived from  $\beta$  or  $I$ , which are much more consistent with each other than in the case of an expanding jet ( $-1.94 \pm 0.10$  vs.  $-2.22 \pm 0.03$  for transition to NRP against  $-1.33 \pm 0.03$  vs.  $-1.94 \pm 0.10$  for an expanding jet) [179]. Assuming the NRP model, from the break time estimate, a high ambient gas density is inferred ( $\sim 10^6 \text{ cm}^{-3}$  [179]), which could be consistent with the fact that a Comptonized component is needed by the X-ray afterglow spectral data (see Section 2.2).

The existence of high temporal indices ( $\beta \leq -1.8$ , see Table 2) has also been taken as evidence for beamed emission (GRB980519 [151]) or for a transition to NRP (GRB000926 [132]). However, in the case of GRB980519, the X-ray data are consistent with a spherical expansion (see Fig. 2), and in the case of the GRB000926 afterglow, the observational scenario appears more complex. By combining together optical and X-ray observations, two breaks are apparent [132]. Piro et al. [132] interpret the early break as due to a relativistic transition from a spherical to a jet-like phase, and the later break as due to the transition of the jet to NRP [87]. This interpretation implies

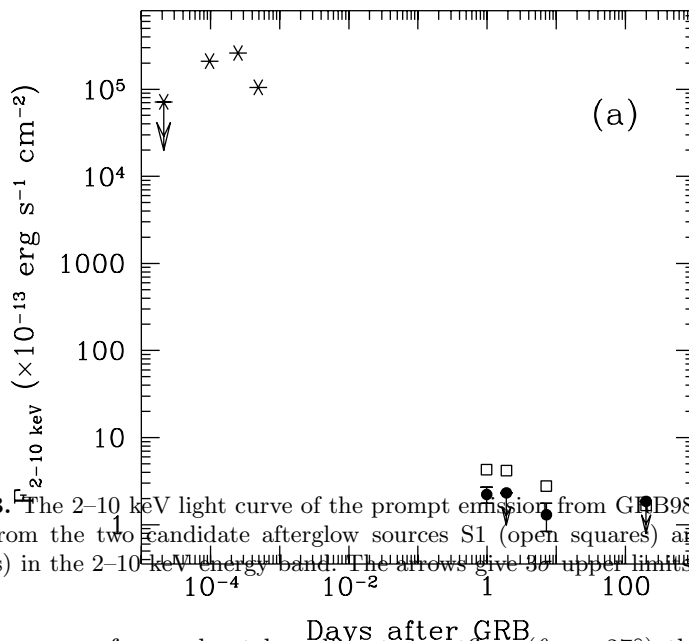


**Fig. 3.** The 2–10 keV light curve of the prompt emission from GRB980425 (stars) and from the two candidate afterglow sources S1 (open squares) and S2 (filled circles) in the 2–10 keV energy band. The arrows give 90% upper limits [121].

the presence of a moderately collimated outflow ( $\theta_c \approx 27^\circ$ ) that expands in a dense medium ( $n \approx 4 \times 10^4 \text{ cm}^{-3}$ ). Unfortunately the derived medium density is much higher than that ( $n \sim 30 \text{ cm}^{-3}$ ) inferred from the broad band spectrum [64], as discussed in Section 2.2. Also, in the case of GRB010222 a late break could be the explanation of the inconsistency of the *BeppoSAX* light curve with the *CHANDRA* flux point taken 9 days after the GRB [179].

The presence of beamed emission would help to reduce the dramatic GRB energy problem. While the isotropic gamma-ray energy  $E_{iso}(\gamma)$  ranges from  $5 \times 10^{51}$  to  $3 \times 10^{54}$  ergs (see e.g., [4,11,154]), the  $E_\gamma$  for a jet with opening angle  $\theta_c$  would be a factor of  $2/\theta_c^2$  lower. Frail et al. [42] attribute the range of variation of  $E_{iso}(\gamma)$  to a range of jet cone angles and give an estimate of the mean value of  $E_\gamma \sim 5 \times 10^{50}$  ergs, where a conversion efficiency of the jet kinetic energy into electromagnetic radiation of 0.2 is assumed [59]. Rossi et al. [144] assume a jet as well, but with a variation in the output energy which depends on the offset angle from the jet axis ( $\propto \theta^{-2}$ ) and attribute the dispersion in the  $E_{iso}(\gamma)$  energy to differences in the jet axis-to-observer viewing angles.

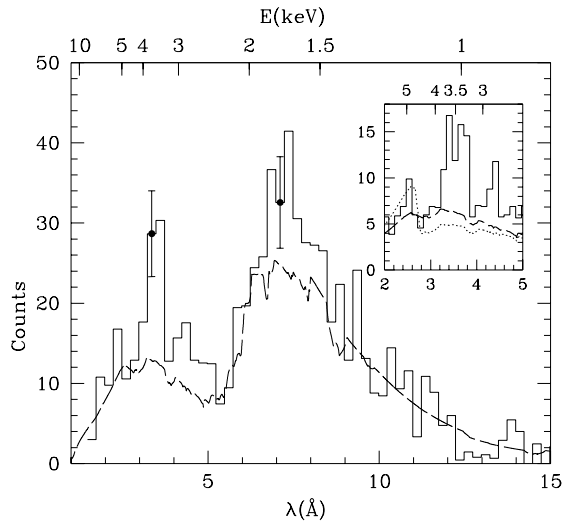
The afterglow of GRB980425 deserves a separate discussion, because of its large impact on the GRB–supernova connection issue. The GRB occurred at a time and in a position which are both consistent with those of the peculiar Type Ic supernova SN1998bw in the nearby galaxy ESO 184-G82 ( $z = 0.0085$ ) [50,75,79]. Following the detection with *BeppoSAX WFCs* and *GRBM* (see Table 1), a prompt X-ray observation of the GRB error box

led to the discovery of two weak sources, S1 and S2, within the *WFC* error box, one of which, S1, was consistent with the SN1998bw position [121]. The 2–10 keV flux level of S2, about two times lower than that of S1, was at the sensitivity limit of the *BeppoSAX MECS* telescopes so that even very small variations of this source could lead to a positive detection or an upper limit. Indeed, the source was no longer detected one day after the first observation and it was barely detectable again 6 days later. Finally, it was not detected during an observation in November 1998 (see Fig. 3). The source S1 was stronger, but showed a very weak power-law fading with index  $\beta = -0.2$ . Neither S1 nor S2 showed "typical" fading behaviour, illustrating the peculiar nature of the burst and afterglow. Further observations of the GRB980425 field with more sensitive X-ray instrumentation are of key importance. An observation performed with XMM-Newton [123] has shown that the X-ray flux from S1 has further faded from the last *BeppoSAX* observation according to an exponential law, while S2, still visible, is the superposition of more sources, likely AGNs.

#### 2.4 Emission/Absorption Features in the X-Ray Spectra

Evidence of emission features has been reported in the X-ray afterglow spectra of GRB970508 [128], GRB970828 [176], GRB991216 [131], and GRB000214 [8]<sup>1</sup>. Table 3 summarizes the major properties of these features and Fig. 4 shows one of the two features discovered in the GRB991216 X-ray afterglow. A feature at 3.5 keV (97% confidence level) was observed from GRB970508 only during the first part (10 hrs) of the follow-up observation of this burst, before a delayed outburst occurred in both the X-ray and optical bands [127]. Also in the case of GRB970828 an emission feature at 5 keV (confidence level of 98.3%) was observed for a limited time duration ( $\sim 5.5$  hrs) during a flare activity of the GRB afterglow. The two emission features from the GRB991216 afterglow ( $4.7\sigma$  excess above the continuum emission at 3.5 keV,  $2\sigma$  excess for the feature at 4.4 keV) were detected for the entire observation duration (3.4 hrs) performed 37 hrs after the main event with *CHANDRA*. In the last case (GRB000214), the continuum level was observed to fade while the emission feature at 4.7 keV ( $3\sigma$  significance level) remained stable for the entire duration of the observation ( $\sim 29$  hrs). Taking into account that three of these GRBs have host galaxies with known redshifts (0.835 for GRB970508 [102], 0.9578 for GRB970828 [34] and 1.02 for GRB991216 [169]), the line features in their respective co-moving frames are consistent with Fe fluorescence lines (Fe I–Fe XX K $\alpha$  line in the case of GRB970508, Fe K line of H-like ions in the case of the lower energy line from GRB991216) or Fe recombination edges (recombination of Fe H-like ions for both the line feature from

<sup>1</sup> After this paper was written, evidence of 5 emission features from GRB011211 (Mg XI, Si XIV, S XVI, Ar XVIII, Ca XX) were reported [139], but their reality is questioned [16,145].



t

**Fig. 4.** Spectrum of the X-ray afterglow of GRB991216 obtained with the *CHANDRA* high energy gratings. The  $4.7\sigma$  excess at 3.5 keV is apparent. In the inset the fine structure of the line is shown [131].

GRB970828 and the higher energy feature from GRB991216). In the case of GRB000214, for which the redshift is not known, if the feature is interpreted as an Fe K fluorescence line, the implied redshift of the GRB source ranges from 0.37 to 0.47, depending on the ionization status of Iron, from neutral to hydrogen-like Fe, respectively.

Independent of the specific identification, all the detected lines point to the presence of ionized Fe at the time of the afterglow measurements, with the ionizing radiation likely due to the GRB flash. The line widths (see Table 3) are not accurately determined except in the case of the 3.5 keV line from GRB991216 (see Fig. 4). In this case the line width has been interpreted [131] as being of kinematic origin, implying velocities of the line emitting material of  $\sim 0.1c$ . This velocity would also be that of the material ejected by the GRB progenitor (if a supernova) a few months before the main GRB event. The large equivalent widths of the lines favour a reflection geometry for the line emitting material [167]. Indeed, for a reflection process the ionizing flux is always efficiently reprocessed into line photons by the outermost Fe layer (optical depth  $\tau_{Fe} \sim 1$ ), while for a transmission process an efficient re-processing of the ionizing flux would require a particular tuning of the density of both the scattering material and free electrons. The amount of Fe needed mainly depends on the density of the scattering cloud and on its distance from the GRB site. In the reflection model worked out by Vietri et

al. [167], the required iron mass to obtain the observed line fluxes is significant (a sizable fraction of a solar mass in the case of GRB991216) which is not expected even for the largest known stars. Only a supernova remnant could contain so much iron. However in the model by Rees and Mészáros [138], in which a continuing (hrs to days) power output after the burst in a magnetohydrodynamic (MHD) wind is required, it is the interaction of this wind with the walls of a funnel previously created by the GRB itself (assumed to be produced in a collapsing star) that gives rise to the emission features. They result from a reprocessing of part of the wind luminosity by a thin layer of the funnel. In this case, the iron mass needed to obtain the line flux is much lower ( $\sim 10^{-8} M_{\odot}$  for GRB991216), thanks to the high material density and the high recombination rate of the Fe ions. In this model the GRB environment is not required to be enriched in Fe by a previous supernova explosion. In a later paper, Mészáros and Rees [104] proposed a different model for the emission line in which the total amount of Fe is significantly larger ( $\sim 10^{-5} M_{\odot}$ ). Here, a hypernova progenitor releases a relativistic shock when the inner black hole is sufficiently powerful to drive the shock progress into the outlying star layers. The heated matter (heavily contaminated by the Fe nuclear matter), which is not accelerated to relativistic energies, expands outside the main body of the star in a cocoon and produces the Fe line thermally.

In this context, the discovery of a transient absorption feature (13 s duration) at 3.8 keV in the prompt emission of GRB990705 [3] could provide an important datum for settling the issue of the Fe abundance and its mass and location within the environment in which the emission lines are produced. Assuming that the observed absorption feature was due to a redshifted Fe K-edge [3] (consistent with the optical redshift  $z_{opt} = 0.8424 \pm 0.0002$  of the GRB host galaxy [86]), the derived Fe abundance ( $A_{Fe} \sim 75$ ) is typical of a supernova remnant (SNR) and its transient nature could be a consequence of its photoionization by the GRB photons. From the estimated column density, supposing a uniform distribution of SNR material, its distance from the GRB site was estimated to be  $\sim 0.1$  pc. Such a short distance makes it very likely that the GRB site was coincident with that of a supernova explosion. The time for the remnant to grow to this size was estimated as  $\sim 10$  yrs. A drawback of this scenario [15,84] is the huge amount of Iron (tens of solar masses) required, unless the absorbing iron is clumped and a clump is by chance along the line of sight.

Lazzati et al. [84] propose an alternative model that does not require a large Fe mass. In this model the assumption is that the quasi-complete ionization of iron is achieved in a much shorter time than the duration of the feature (13 s), which is due to resonant scattering of the GRB photons off H-like iron (transition 1s-2p,  $E_{rest} = 6.927$  keV), while its disappearance is due to a halt of the electron recombination by an electron temperature increase. In this model, to fit the data, a Fe relative abundance  $\sim 10$  times the solar value and an Fe mass of  $\sim 0.2 M_{\odot}$  are required. Also in this model,

an iron rich environment, typical of an SNR, is required and the distance to the absorbing iron is low ( $\sim 2 \times 10^{16}$  cm). As a consequence, independent of the specific model, a SN explosion preceding the GRB event is required, which is likely to be associated with the GRB event itself. In this framework, the afterglow emission features appear when the strong ionizing flux has decreased and electron recombination restarts.

### 3 The Early X-Ray Afterglow

A peculiar property of the X-ray afterglow light curves is their very smoothly fading behaviour, except in a few cases in which an outburst (GRB 970508), a flaring activity (GRB 970828), and a rise from below the *BeppoSAX MECS* sensitivity (GRB 981226), were observed [47,127,176]. By comparison, the time profile of the prompt  $\gamma$ -ray emission is erratic and even spiky. In order to explain the complex time profiles of GRBs, it has been hypothesized [78,147,148] that the GRB itself could be due to internal shocks, with fast-rise exponential-decay (FRED) events perhaps also involving external shocks [31]). However, there is a general consensus that the late afterglow emission is likely due to external shocks (see, e.g. [101,150]). In this scenario, the two phenomena can evolve in different ways and can involve energetics which are not necessarily correlated. It has also been suggested [149,152] that the early afterglow could start already only a few tens of seconds after the burst. In fact, in a few cases like GRB970228 [23,26] and GRB970508 [127], the extrapolation of the 2-10 keV afterglow fading law back to the time of the GRB main event gives a flux consistent with that measured during the last portion of the event. Using the ratio between the 2-10 keV fluence of the last portion of the prompt emission and that of the late afterglow, Frontera et al. [48] demonstrated that this property is valid also for an entire sample of GRBs with known afterglows; approximately the second half of the GRB prompt X-ray emission is strictly correlated with the afterglow emission. This suggests that at least the tail of the GRBs can be due to afterglow emission, while at the onset of the primary event this contribution is negligible. Once the rise of the afterglow has been established, the framework of the fireball model permits the initial Lorentz factor  $\Gamma_0$  of the shocked ambient medium to be evaluated [152]. From the above results  $\Gamma_0 \sim 150$  for all GRB events investigated, except for GRB980425 in which a much lower value ( $\Gamma_0 < 50$ ) is found [48].

At higher energies ( $> 10$  keV), as mentioned in Section 2.2, late afterglow emission has been discovered only from GRB990123 with the *BeppoSAX PDS* instrument [69]. However, early afterglow emission is also expected from, e.g., electron-synchrotron self-Inverse Compton and proton-synchrotron processes [153,180] and some evidence of a possible early, high energy afterglow has been reported [20,22,55]. The most suggestive result is that found by Giblin et al. [55] with the strong *BATSE* event GRB980923 in the 25–300 keV range. The

*BATSE* data show a GRB light curve which, after 40 s of erratically variable flux, smoothly decays with a power-law shape of index  $\beta \sim -1.8$  for about 400 s until the event becomes invisible. Correspondingly, the energy spectrum shows a power-law shape with a photon index  $I$ , which, after 40 s from the GRB onset, exhibits a jump from -1 to -1.7, which is typical of the X-ray afterglow photon indices (see Section 2.2).

## 4 Open Issues and Future Prospects

In spite of the tremendous advances in the years since the discovery of the first X-ray afterglows, many questions about the GRB phenomenon are still open which can only be answered with further X-ray observations. Analysis of the afterglow radiation seems to indicate a synchrotron origin, but in some cases multiwavelength spectra (see Section 2.2) show the presence of an additional component in the X-ray band interpreted as electron self-Inverse Compton radiation. It is important to obtain good quality, multiwavelength spectra for a large sample of GRBs to determine the relevant emission mechanisms of the afterglow radiation.

Breaks in the X-ray afterglow light curves have been observed for a few GRB afterglows, while at longer wavelengths such breaks are more frequent [42]. The jet model predicts that these breaks are achromatic if the jet propagates into a medium with uniform density. However, if the jet moves into a wind-like circumstellar environment ( $\rho \propto r^{-s}$  with  $s \approx 2$ ), the break is expected to be less relevant in X-rays than in the optical band [80]. In addition, other models have been proposed for interpreting such breaks (e.g., transition to NRP, see Section 2.3). Thus it is of key importance to measure X-ray afterglow light curves with high statistical quality in order to test the jet model and to derive the ambient medium properties to be compared with the properties derived from the multiwavelength spectra.

The ambient medium density, along with other GRB environmental properties (composition, velocity, temperature, metal abundance) can also be inferred from the detection of X-ray lines or edges in the spectra of the prompt and delayed X-ray emission. This information is important for determining the nature of the GRB progenitor, which is one of the most debated issues in astrophysics today. For the case of collapse of a massive progenitor, the GRB environment is expected to be Fe polluted and line features are more likely. On the contrary in a clean environment such as that expected for neutron star mergers, Fe lines are not likely. The X-ray lines detected so far point toward the presence of a medium highly ionized by the GRB main event, with iron abundance higher than solar. It is likely that this iron is produced and ejected by the GRB progenitor before the burst, which supports the hypothesis a supernova-like explosion (hypernova, collapsar or supranova [116,166,175]). However many questions are still open even in this scenario. For example:

- Why do we not see any absorption feature in the prompt emission of the GRBs which show an emission feature during the afterglow phase (GRB970508 or GRB000214)?
- Why are the emission lines in the afterglow spectra of GRB970508 and GRB970828 observed only for a limited amount of time, while in the case of GRB000214 the line is stable?
- Why in many other GRBs observed with *BeppoSAX* do we not see any feature?
- Is this due to the limited sensitivity of the *BeppoSAX* instrumentation or is it due to an intrinsic physical process?

Only more sensitive and continuous observations of GRBs from the main event through to the late afterglow can answer these questions.

High quality light curves of the GRB prompt emission and afterglows, with no interruption, could also resolve the issue of the onset time of the afterglow emission phase, its time profile and its spectral evolution. This information is of key importance to study the feedback of the intense  $\gamma$ -ray flux on the dynamics of the fireball and on the afterglow emission properties [10,103,163]. High quality light curves at multiple wavelengths could definitely settle the question of the rate of GRBs with single or multiple broken power-law temporal behaviour. If the breaks in the light curve imply the presence of jets, the GRB energetic problem could be solved, or mitigated, and ordinary supernovae could be energetic enough to be the origin of GRB events [42]. High quality light curves would also permit the study of short time variations in the afterglow fading, and thus of the degree of homogeneity of the circumburst medium [47].

Another open issue concerns the origin of short ( $<1$  s) GRB events. Until now, no prompt (within few hrs) follow-up of these events has been possible and no afterglow source has ever been identified [73]. A claim for the detection of a transient (100 s duration) and fading hard X-ray emission, obtained by summing the *BATSE* light curves of a sample of 76 short GRBs has recently been reported (see [85], but also [22]). Lazzati et al. [85] interpret this emission as possible evidence for afterglows from short GRBs. This claim still has to be confirmed by other, more sensitive observations and its origin is not clear. It could also be prompt emission from truly long GRBs with have a spectrally hard, short and strong pulse at their onset, and a long tail which is not individually observable because it is below the sensitivity limit of the instrumentation used. More sensitive GRB observations with immediate position identification are needed to disentangle the short GRB origin issue and the afterglow properties of these events.

The cause of "dark" GRBs (see also the chapter by E. Pian) is still a mystery. A possible explanation is the presence of dust in the environment around GRB sites that obscures the optical emission, even if the GRB output may be enough to destroy the dust in the immediate surroundings [33]. Observations of X-ray lines from these GRBs could be crucial for stabil-



ishing the environmental properties. However other possibilities cannot be excluded, such as a rapid decline of the optical light or a high redshift of the object. Only fast afterglow searches, starting minutes after the main event with multiple wavelength coverage of the afterglow emission, can definitely settle this issue.

The X-ray flashes detected with *BeppoSAX* [68] with no  $\gamma$ -ray counterparts are still a mystery. They could be GRBs at very high redshifts ( $z > 10$ ) or GRBs with very soft spectra, or GRBs from fireballs with a low Lorentz factor. More sensitive observations of these events are needed.

The fireball model of GRBs is currently the most successful for interpreting the X-ray data. Other models have been proposed, such as the cannonball (see, e.g., [29]) and only future observations will be able to distinguish between, and determine the validity of, these alternative models.

One of the major limitations of the current investigations on GRB afterglows is the delay from the main event to the follow-up observations. Many of the issues discussed herein will be solved when future missions, now under development (in particular *Swift Gamma-Ray Burst Explorer (Swift)* [53] and *Gamma-Ray Large Area Space Telescope (GLAST)* [52]) are operating. *Swift* will perform immediate ( $\sim 1$  min) follow-up observations in the X-ray and optical bands and will trigger very prompt optical, near-infrared, and radio observations with ground-based telescopes. The  $\gamma$ -ray mission *GLAST* will allow a sensitive and high time resolution study of the highest energies (GeV) emitted by GRBs and other missions, like the European *International Gamma-Ray Astrophysics Laboratory (INTEGRAL)* (see, e.g., [97]) and the Italian *Astro-rivelatore Gamma a Immagini LEggero (AGILE)* [161] are expected to make key contributions to the resolution of the GRB mystery.

## 5 Acknowledgments

I wish to thank Lorenzo Amati for his generous contribution to the preparation of the Tables 1 and 2 of this paper, Mario Vietri for his very useful comments and suggestions for improving the paper, and Nicola Masetti and John Stephen for their careful reading of the manuscript. I also wish to thank the colleagues of the *BeppoSAX* team (L. Amati, C. Guidorzi, L. Nicastro, L. Piro, P. Soffitta), who have permitted the publication of preliminary results. Many thanks especially to my wife for her sympathy for my days of work at home for this chapter, when I should have been available for family needs. I also like to acknowledge financial support from the *Italian Space Agency (ASI)* and from the Ministry of the University of Italy (COFIN funds).

**Table 1.** GRBs Observed for X-rays Afterglows

GRB	Instr. Error for box GRB radius loc. <sup>a</sup>	Start of X-ray follow- up <sup>b</sup>	Instr. for follow- up <sup>c</sup>	X-ray counterpart flux at start <sup>d</sup> (erg cm <sup>-2</sup> s <sup>-1</sup> )	Source name <sup>e</sup>	Error box radius <sup>e</sup>	Ref.
970111	WFC 3'	16.5	NFI	$< 1.6 \times 10^{-13}$	1SAXJ1528.1+1937(?)		[35]
970228	WFC 3'	8.27	NFI	$3.2 \times 10^{-12}$	1SAXJ0501.7+1146	50"	[23]
		....	HRI	$\sim 2 \times 10^{-12}$	RXJ050146+1149.9	10"	[44]
970402	WFC 3'	8.39	NFI	$2.7 \times 10^{-13}$	1SAXJ1450.1-6920	50"	[109]
970508	WFC 1.9'	5.6	NFI	$\sim 7 \times 10^{-13}$	1SAXJ0653.8+7916	50"	[127,128]
970616 <sup>f</sup>	BAT 2°	4.0	PCA	$1.1 \times 10^{-11}$	01 18 57 -05 28 00	0.7' × 18'	[90]
970815	ASM 6'×3'	76.8	HRI	$< 1.0 \times 10^{-13}$			[57]
970828	ASM 2.5'×1'	3.6	PCA	$1.15 \times 10^{-11}$	18 08 32.2 +79 16 02	30"	[91,106,107,176]
971214	WFC 3.3'	6.55	NFI	$\sim 7 \times 10^{-13}$	1SAXJ1156.4+6513	60"	[30]
971227	WFC 8'	14.4	NFI	$2.6 \times 10^{-13}$	1SAXJ1257.3+5924	90"	[6]
980329	WFC 3'	7.0	NFI	$1.4 \times 10^{-12}$	1SAXJ0702.6+3850	50"	[177]
980425	WFC 8'	10.2	NFI	$4.0 \times 10^{-13}$	1SAXJ1935.0-5248	90"	[121]
980515	WFC 4'	9.83	NFI	$1.6 \times 10^{-13}$	1SAX J2116.8-6712	90"	[36]
980519	WFC 3'	4.74	NFI	$6.0 \times 10^{-13}$	1SAXJ2322.3+7716	50"	[110,111]
980613	WFC 4'	8.63	NFI	$3.3 \times 10^{-13}$	1SAXJ1017.9+7127	50"	[24,157]
980703	ASM 4'	22.0	NFI	$4.7 \times 10^{-13}$	1SAXJ2359.1+0835	50"	[168]
980706 <sup>g</sup>	COM 4°	2.7	PCA	$4.0 \times 10^{-11}$			[92,165]
981226 <sup>h</sup>	WFC 6'	11.3	NFI	$< 1.5 \times 10^{-13}$	1SAXJ2329.6-2356	60"	[47]
990123	WFC 2'	5.8	NFI	$1.6 \times 10^{-11}$	1SAXJ1525.5+4446	50"	[67,69]
990217	WFC 3'	6.5	NFI	$< 1.0 \times 10^{-13}$			[129]
990506	BAT 9.6'	3.0	PCA	$3.2 \times 10^{-11}$	11 54 46 -26 45 35	6'	[72]
990510	WFC 3'	8.0	NFI	$5.2 \times 10^{-12}$	1SAXJ1338.1-8030	56"	[81]
990627	WFC 3'	8.0	NFI	$3.5 \times 10^{-13}$	1SAXJ0148.5-7704	69"	[112]
990704	WFC 7'	8.3	NFI	$8.0 \times 10^{-13}$	1SAXJ1219.5-0350	60"	[38]
990705	WFC 3'	11.38	NFI	$1.9 \times 10^{-13}$	1SAXJ0509.9-7207	120"	[3]
990806	WFC 3'	7.77	NFI	$4.0 \times 10^{-13}$	1SAXJ0310.6-6806	60"	[46,105]
990907 <sup>i</sup>	WFC 6'	10.98	NFI	$1 - 2 \times 10^{-12}$	1SAXJ0731.2-6928	180"	[130]
991014	WFC 6'	11.76	NFI	$4.0 \times 10^{-13}$	1SAXJ0651.0+1136	90"	[178]
991106 <sup>j</sup>	WFC 3'	7.8	NFI	$1.25 \times 10^{-13} ?$	1SAXJ2224.7+5423 ?	90"	[7]
991216	BAT 1.1°	4.03	PCA	$1.24 \times 10^{-10}$	05 09 31.5 +11 17 05.7	1.5"	[131,160]
000115	BAT 1.7°	2.92	PCA	$4.3 \times 10^{-11}$	08 03 12 -17 05 59	18'	[93]
000210	WFC 2'	7.2	NFI	$4.5 \times 10^{-13}$	01 59 15.7 -40 39 32.3	1.6"	[25,54,134]
000214	WFC 6.5'	12.0	NFI	$7.7 \times 10^{-13}$	1SAXJ1854.4-6627	50"	[8]
000528 <sup>k</sup>	WFC 2'	8.3	NFI	$1.8 \times 10^{-13}$	1SAXJ1045.1-3359	90"	[82]
000529 <sup>l</sup>	WFC 4'	7.5	NFI	$2.8 \times 10^{-13}$	1SAXJ0009.8-6128	120"	[37]
000615 <sup>m</sup>	WFC 2'	10.04	NFI	$6.7 \times 10^{-14}$	1SAXJ1532.4+7349	120"	[113]
000926	IPN 3'×10'	48.96	NFI	$3.8 \times 10^{-13}$	17 04 01.6 +51 47 08.6	2"	[64,132]
001025 <sup>n</sup>	IPN 5'	45.60	XMM	$1 - 2 \times 10^{-13}$	08 36 35.42-13 04 09.9	<10"	[1,2]
001109	WFC 2.5'	16.5	NFI	$7.1 \times 10^{-13}$	1SAXJ1830.1+5517	50"	[5]
010214	WFC 3'	6.28	NFI	$1.0 \times 10^{-12}$	1SAXJ1741.0+4834	60"	[60]
010220	WFC 4'	16.0	NFI	$< 1.0 \times 10^{-13}$			[89]
010222	WFC 2.5'	8.0	NFI	$1.2 \times 10^{-11}$	1SAXJ1452.2+4301	30"	[180]
011121	WFC 2'	21.25	NFI	$\sim 1.0 \times 10^{-12}$	1SAXJ113426-7601.4	50"	[133,135]
011211 <sup>o</sup>	WFC 1'	11.13	XMM	$1.9 \times 10^{-13}$	11 15 17.9-21 56 57.5	<10"	[139]

**Table 1.** (continued)

- <sup>a</sup> *WFC* on board *BeppoSAX*; *BAT* = *BATSE* on board *CGRO*; *ASM* on board *RXTE*; *COM* = *COMTEL* on board *CGRO*; *IPN* = InterPlanetary Network.
- <sup>b</sup> Earliest afterglow search, in hours from the GRB detection.
- <sup>c</sup> Instrument used for the earliest afterglow search: *NFI* on board *BeppoSAX*; *HRI* on board *ROSAT*; *PCA* on board *RXTE*; *XMM* = *XMM-Newton* satellite.
- <sup>d</sup> Energy band: 2-10 keV. All upper limits are  $3\sigma$  except for GRB981226 which is  $2\sigma$ .
- <sup>e</sup> The best available coordinates and error box radius. When no source name is available, we report here the equatorial coordinates  $\alpha_{J2000}$ ,  $\delta_{J2000}$ , when available.
- <sup>f</sup> No more sensitive follow-up of this source is available. No decay was observed. No detection of radio or near infrared (NIR) afterglow was obtained ([56,58,172]).
- <sup>g</sup> It is unclear whether this flux was due to the afterglow. After 1.5 hrs from the first detection the source was no longer visible [92]. This would imply a decay index  $\beta < -3$ . Most likely, the *PCA* source is not related to the GRB [165].
- <sup>h</sup> The source was not visible at the beginning of the observation campaign. Afterward, the source flux increased by more than a factor of 3 in about 10000 s. Then the source started fading.
- <sup>i</sup> Due to technical problems, the *BeppoSAX* observation had a duration of only 20 min. The probability of a serendipitous source is  $\sim 3 \times 10^{-3}$  [130].
- <sup>j</sup> The source fading was not observed. The probability of detecting an unrelated foreground source at this flux level or higher, in the GRB error box given by the *BeppoSAX* WFCs (see GCN 435) is about 10%.
- <sup>k</sup> The source faded to a  $2\sigma$  upper limit of  $5.0 \times 10^{-14}$  erg cm<sup>-2</sup> s<sup>-1</sup> after 78.86–99.06 hrs from the GRB onset.
- <sup>l</sup> The source was undetected ( $2\sigma$  upper limit of  $1.3 \times 10^{-13}$  erg cm<sup>-2</sup> s<sup>-1</sup>) 17 hrs after the main event.
- <sup>m</sup> Flux in the 1.6–4 keV band. The source was undetected ( $2\sigma$  upper limit of  $3.0 \times 10^{-14}$  ergs cm<sup>-2</sup> s<sup>-1</sup>) after 20 hrs from the GRB event. This might be a field source unrelated to the GRB.
- <sup>n</sup> Flux in the 0.5-10 keV band.
- <sup>o</sup> Flux in the 0.2-10 keV band.

**Table 2.** X-ray Afterglow Properties

GRB	Temporal index $\beta$	Photon index I	$n_H / n_H^G$ ( $\times 10^{21} \text{ cm}^{-1}$ )	2–10 keV flux at $10^5 \text{ s}^a$ ( $\text{erg cm}^{-2} \text{ s}^{-1}$ )	Redshift z	Ref.
970111	$< -1.5$ ( $3\sigma$ )	...	...	$< 1.0 \times 10^{-13}$	...	[35]
970228	$-1.33_{-0.13}^{+0.11}$	$-2.06 \pm 0.24$	$3.5_{-2.3}^{+3.3} / 1.6$	$\sim 6.8 \times 10^{-13}$	0.695	[23,45]
	$-1.50_{-0.23}^{+0.35}$	$-2.1 \pm 0.3$	$3.5_{-2.3}^{+3.3} / 1.6$	$\sim 1.1 \times 10^{-12}$	...	[44]
970402	$-1.3-1.6$	$-1.7 \pm 0.6$	$< 20 / 2.0$	$\sim 4.5 \times 10^{-14}$	...	[109]
970508	$-1.1 \pm 0.1^b$	$-1.5 \pm 0.8^c$	$6.0_{-5.5}^{+13} / 0.5$	$3.5 \times 10^{-13d}$	0.835	[127,128]
		$-2.2 \pm 0.7^e$	$0.5_{-0.5}^{+5} / 0.5$	$1.5 \times 10^{-12f}$		
970828	$-1.44 \pm 0.07$	$[-2]^g$	$4.1_{-1.6}^{+2.1} / 0.34^h$	$6.0 \times 10^{-13}$	0.9758	[34,90,91]
971214	$-0.85_{-0.15}^{+0.17}$	$-1.6 \pm 0.2$	$1.0_{-1.0}^{+2.3} / 0.6$	...	3.42	[30]
971227	$-1.12_{-0.08}^{+0.05}$	$[-2.1]$	$[0.13] / 0.13$	$\sim 1.4 \times 10^{-13}$	...	[6]
980329	$-1.35 \pm 0.03$	$-2.4 \pm 0.4$	$10 \pm 4 / 0.9$	$2.0 \times 10^{-13}$	$< 3.9$	[33,71,177]
980425 <sup>i</sup>	$-0.16 \pm 0.04$	$-2.0 \pm 0.3$	$[0.39] / 0.39$	$\sim 4.0 \times 10^{-13}$	0.0085	[121]
980519	$-1.83 \pm 0.30$	$-2.8_{-0.6}^{+0.5}$	$3-20 / 1.73$	$8.0 \times 10^{-14}$	...	[111]
980613	$-1.19 \pm 0.17$	$> -2.4 ?$	...	$\sim 2.3 \times 10^{-13}$	1.097	[24,157]
	$-1.05 \pm 0.37^j$	...	...	...	...	[14,70]
980703	$< -0.91$ ( $3\sigma$ )	$-2.51 \pm 0.32$	$36_{-13}^{+22} / 0.34^k$	$4.5 \times 10^{-13}$	0.966	[168]
981226	$-1.31_{-0.44}^{+0.39l}$	$-1.92 \pm 0.47$	$[0.18] / 0.18$	$\sim 2.0 \times 10^{-13}$	...	[47]
990123	$-1.44 \pm 0.07$	$-1.86 \pm 0.1^m$	$0.51_{-0.1}^{+0.7} / 0.21$	$1.25 \times 10^{-12}$	1.600	[67,69]
990510	$-1.42 \pm 0.07^n$	$-2.03 \pm 0.08$	$2.1 \pm 0.6 / 0.94$	$9.6 \times 10^{-13}$	1.619	[81,122]
990627	$-1.741_{-0.55}^{+0.63}$	$-2.8 \pm 0.7$	$[0.52] / 0.52$	$< 1.6 \times 10^{-13}$	[5]	
990704	$-0.83 \pm 0.16$	$-1.691_{-0.60}^{+0.34}$	$[0.3] / 0.3$	$\sim 3.3 \times 10^{-13}$	...	[38]
990705 <sup>o</sup>	$-1.58 \pm 0.06^p$	...	...	$< 1.2 \times 10^{-13}$	0.86	[3]
990806	$-1.2 \pm 0.3$	$-2.161_{-0.61}^{+0.50}$	$[0.35] / 0.35$	$\sim 2.0 \times 10^{-13}$	...	[105]
991014 <sup>q</sup>	$< -0.4$ ( $3\sigma$ )	$-1.53 \pm 0.25$	$[2.5] / 2.5$	$\sim 3.0 \times 10^{-13}$	...	[178]
991216	$-1.62 \pm 0.07$	$-2.2 \pm 0.2^r$	$3.51_{-1.5}^{+1.5} / 2.1$	$\sim 5.0 \times 10^{-12}$	1.02	[62,131,160]
000115	$< -1.0$	...	...	$< 1.0 \times 10^{-11}$	...	[93]
000214	$-0.8 \pm 0.5$	$-2.0 \pm 0.3^s$	$0.071_{-0.07}^{+0.75} / 0.55$	$\sim 5.0 \times 10^{-14s}$	0.37-	[8]
	$-1.41 \pm 0.03^p$	...	...	...	$0.47^t$	
000926	$-1.89_{-0.19}^{+0.16u}$	$-1.85 \pm 0.15^v$	$4.0_{-2.5}^{+3.5w} / 0.27$	$9.0 \times 10^{-13}$	2.06	[64,132]
	$-1.70 \pm 0.16^x$	$-2.23 \pm 0.3^y$	$[4.0]^w / 0.27$	...	...	
001109	$-1.18 \pm 0.05^p$	$-2.4 \pm 0.3$	$8.7 \pm 0.4 / 0.42$	$\sim 8.0 \times 10^{-13}$	...	[5]
010214	$-2.1_{-1.0}^{+0.6}$	$-1.3_{-0.8}^{+0.6}$	$[0.27] / 0.27$	...	...	[60]
	for $t > 8$ hrs					
	$-0.99_{-0.04}^{+0.09}$					
	for $t < 8$ hrs					
010222	$-1.33 \pm 0.04^z$	$-1.97 \pm 0.05$	$1.5 \pm 0.3 / 0.16$	$2.4 \times 10^{-12}$	1.477	[179]
	for $t > 8$ hrs					
	$\sim 0.8^p$					
	for $t < 8$ hrs					

**Table 2.** (continued)

- <sup>a</sup> All upper limits are  $3\sigma$  except for GRB990627 and GRB990705 which are  $2\sigma$ .  
<sup>b</sup> from  $6 \times 10^4$  s to  $5.8 \times 10^5$  s an X-ray outburst occurred with integrated energy excess with respect to the power-law decay equal to  $\sim 5\%$  that of the GRB primary event. The outburst was also visible at optical wavelengths (see references in [127]).  
<sup>c</sup> Index measured before the outburst. During the outburst the slope is variable [127].  
<sup>d</sup> Interpolated from the data before and after the outburst.  
<sup>e</sup> Index measured soon after the outburst.  
<sup>f</sup> Interpolated taking into account the outburst data.  
<sup>g</sup> Evidence of an emission feature (see Section 2.4).  
<sup>h</sup>  $n_H$  measured in the latest observation period.  
<sup>i</sup> Assuming that the source S1 is coincident with SN1998bw position (see Section 2.3).  
<sup>j</sup> Result reported by [14].  
<sup>k</sup>  $n_H$  value corrected for redshift.  
<sup>l</sup> Temporal index during the fading phase of the source. See note h of Table 1.  
<sup>m</sup> The afterglow is visible up to 60 keV with a power-law spectrum.  
<sup>n</sup> Comparing the prompt emission with the X-ray afterglow emission, Pian et al. [122] derive the presence of a break in the afterglow light curve which tends, at early and late epochs, to a power-law of index  $\beta \sim -1$  and  $\beta \sim -2$ , respectively, with a break time of  $\sim 0.5$  days, compatible with that determined from the optical light curve [63,74,158].  
<sup>o</sup> The field is highly contaminated by stray radiation.  
<sup>p</sup> Derived by comparing the prompt emission and late afterglow data.  
<sup>q</sup> The shortest event followed by *BeppoSAX* (3.29 s at 40–700 keV).  
<sup>r</sup> Also evidence of two emission lines (see Table 3).  
<sup>s</sup> Extrapolated from the measured light curve.  
<sup>t</sup> Based on X-ray emission feature interpretation (see text).  
<sup>u</sup> *BeppoSAX* plus *CHANDRA* data. Evidence of a discrepancy between optical and X-ray decline rates [132].  
<sup>v</sup> *BeppoSAX* plus *CHANDRA* data 2–3 days after the main event.  
<sup>w</sup> Corrected for redshift [132]. This  $n_H^z$  value was added to the Galactic column density  $n_H^G$ . According to Harrison et al. [64], the  $n_H^z$  is not needed by the *CHANDRA* data.  
<sup>x</sup> From *CHANDRA* data only.  
<sup>y</sup> From *CHANDRA* data 13 days after the GRB.  
<sup>z</sup> The extrapolation of the power-law light curve, derived from the *BeppoSAX* data, is above the X-ray flux measured 9 days after the burst with *CHANDRA* [65,179] (see text).

**Table 3.** Properties of the Detected X-ray Emission Features

Quantity	GRB970508	GRB970828	GRB991216	GRB000214
$E_l$ (keV)	$3.4 \pm 0.3$	$5.04^{+0.23}_{-0.31}$	$3.49 \pm 0.06$ $4.4 \pm 0.5$	$4.7 \pm 0.2$
$FWHM_l$ (keV)	$< 0.5$	$0.73^{+0.89}_{-0.73}$	$0.54 \pm 0.16$ $> 2.35$	$< 0.4$
$F_l^a$ ( $10^{-13} \text{erg cm}^{-2} \text{s}^{-1}$ )	$3 \pm 1$	$1.5 \pm 0.8$	$1.7 \pm 0.5$ $2.7 \pm 1.4$	$0.67 \pm 0.22$
$EW_l$ (keV)	$\sim 1.5$	$\sim 1.8$	$0.5 \pm 0.013$ $\sim 0.8$	$\sim 2.1$
$F_\nu^b$ ( $10^{-12} \text{erg cm}^{-2} \text{s}^{-1}$ )	$\sim 7$	$\sim 0.4$	$\sim 2.3$	$\sim 0.3$
Redshift $z$	0.835	0.9578	1.02	$0.37\text{--}0.47^c$
$E_l^0$ (keV) <sup>d</sup>	$6.24 \pm 0.55$	$9.86^{+0.45}_{-0.61}$	$7.05 \pm 0.12$ $8.9 \pm 1.0$	$6.4\text{--}6.97^b$
$L_l^e$ ( $10^{44} \text{erg s}^{-1}$ )	$6.7 \pm 2.7$	$4.8 \pm 2.5$	$5.7 \pm 1.6$ $9.0 \pm 4.7$	$0.45 \pm 0.15^f$
hrs from GRB <sup>g</sup>	6–16	32–38	37–40	12–41
Mission	<i>BeppoSAX</i>	<i>ASCA</i>	<i>CHANDRA</i>	<i>BeppoSAX</i>
Instrument	<i>NFI</i>	<i>SIS+GIS</i>	<i>Gratings+ACIS-S</i>	<i>NFI</i>
References	[128]	[176]	[131]	[8]

<sup>a</sup> Line flux.

<sup>b</sup> Continuum flux in the 2–10 keV band.

<sup>c</sup> Depends on the Fe ionization state (Fe K X-ray fluorescence assumed).

<sup>d</sup> Energy line corrected for cosmological redshift.

<sup>e</sup> Derived assuming  $H_0 = 65 \text{km/s Mpc}$  and  $q_0 = 0.5$ .

<sup>f</sup> Assuming  $z = 0.47$ .

<sup>g</sup> Time interval during which the line was visible.

## References

1. B. Altieri, N. Schartel, M. Santos, L. Tomas, M. Guainazzi, L. Piro, A. Parmar: GCN 869, (2000)
2. B. Altieri, N. Schartel, D. Lumb, L. Piro, A. Parmar: GCN 884 (2000)
3. L. Amati et al.: Science **290**, 953 (2000)
4. L. Amati et al.: Astron. Astrophys. **390**, 81 (2002)
5. L. Amati et al.: in preparation (2003)
6. L.A. Antonelli et al.: Astron. Astrophys. Suppl. Ser. **138**, 435 (1999)
7. L.A. Antonelli et al.: GCN 445 (1999)
8. L.A. Antonelli et al.: Astrophys J. Lett. **545**, L39 (2000)
9. D. Band et al.: Astrophys J. **413**, 281 (1993)
10. A.M. Beloborodov: Astrophys J. **565**, 808 (2002)
11. J.S. Bloom, D.A. Frail & R. Sari: Astron. J. **121**, 2879 (2001)
12. G. Boella, R.C. Butler, G.C. Perola, L. Piro, L. Scarsi, J.A.M. Bleeker: Astron. Astrophys. Suppl. Ser. **122**, 299 (1997)
13. G. Boella et al.: Astron. Astrophys. Suppl. Ser. **122**, 327 (1997)
14. M. Boer & B. Gendre : Astron. Astrophys. **361**, L21 (2000)
15. M. Boettcher, C.D. Dermer, L. Amati & F. Frontera: in *Gamma Ray Bursts in the Afterglow Era, Proc. International Workshop at Rome, Italy, 17-20 October 2000*, eds. E. Costa, F. Frontera, J. Hjorth (Springer, Heidelberg 2001) p. 160
16. K.N. Borozdin, and S.P. Trudolyubov: Astrophys J. **583**, L57 (2003)
17. J.J. Brainerd: Nature **355**, 552 (1992)
18. M.S. Briggs et al.: Astrophys J. **459**, 40 (1996)
19. T. Bulik, D.Q. Lamb, P.S. Coppi: Astrophys J. **505**, 666 (1998)
20. R.A. Burenin et al.: Astron. Astrophys. **344**, L53 (1999)
21. R.A. Chevalier, Z.-Y. Li: Astrophys J. Lett. **520**, L29 (1999)
22. V. Connaughton: Astrophys J. **567**, 1028 (2001)
23. E. Costa et al.: Nature **387**, 783 (1997)
24. E. Costa et al.: IAUC 6939 (1998)
25. E. Costa et al.: GCN 553, (2000)
26. E. Costa: in *AIP Conference Proc.*, ed. R.M. Kippen, R.S. Malozzi, G.J. Fishman, vol.526, p. 365 (2000)
27. S. Covino et al.: Astron. Astrophys. **348**, L1 (1999)
28. Z.G. Dai, T. Lu: Astrophys J. Lett. **519**, L155 (1999)
29. A.Dar, A. De Rújula: astro-ph/0012227 (2000)
30. D. Dal Fiume et al.: Astron. Astrophys. **355**, 454 (2000)
31. C.D. Dermer, M. Böttcher, J. Chiang: Astrophys J. Lett. **515**, L49 (1999)
32. J.M. Dickey & F.J. Lockman: Ann. Rev. Astron. Astrophys. **28**, 215 (1990)
33. S.G. Djorgovski et al.: in *Proc. IX Marcel Grossmann Meeting*, eds. V. Gurzadyan, R. Jantzen, R. Ruffini (World Scientific, Singapore 2001)
34. S.G. Djorgovski, D.A. Frail, S.R. Kulkarni, J.S. Bloom, S.C. Odewahn, A. Diercks: Astrophys J. **562**, 654 (2001)
35. M. Feroci et al.: Astron. Astrophys. **332**, L29 (1998)
36. M. Feroci, L. Piro, M.R. Daniele, G. Gennaro, S. Rebecchi, G. Celidonio, L.A. Antonelli, J. Heise: IAUC 6909 (1998)
37. M. Feroci et al.: GCN 685 (2000)
38. M. Feroci et al.: Astron. Astrophys. **378**, 441 (2001)

39. G.J. Fishman, C.A. Meegan: *Ann. Rev. Astron. Astrophys.* **33**, 415 (1995)
40. D.A. Frail, S.R. Kulkarni, S.R. Nicastro, M. Feroci, G.B. Taylor: *Nature* **389**, 261 (1997)
41. D.A. Frail et al.: *Astrophys J. Lett.* **538**, L129 (2001)
42. D.A. Frail et al.: *Astrophys J. Lett.* **562**, L55 (2001)
43. F. Frontera, E. Costa, D. dal Fiume, M. Feroci, L. Licastro, M. Orlandini, E. Palazzi, G. Zavattini: *Astron. Astrophys. Suppl. Ser.* **122**, 357 (1997)
44. F. Frontera et al.: *Astron. Astrophys.* **334**, L69 (1998)
45. F. Frontera et al.: *Astrophys J. Lett.* **493**, L67 (1998)
46. F. Frontera, M. Capalbi, M.R. Daniele, E. Montanari, A. Paolino, A. Tesseri, C. Pastor, G. Gandolfi: *IAUC7235* (1999)
47. F. Frontera et al.: *Astrophys J.* **540**, 697 (2000)
48. F. Frontera et al.: *Astrophys J. Suppl.* **127**, 59 (2000)
49. T.J. Galama, R.A.M.J. Wijers, M. Bremer, P.J. Groot, R.G. Strom, C. Kouveliotou, J. Van Paradijs: *Astrophys J. Lett.* **500**, L97 (1998)
50. T.J. Galama et al.: *Nature* **395**, 670 (1998)
51. G. Gandolfi: *GCN 118* (2001)
52. N.A. Gehrels, I. Michelson: *Astropart Phys.* **11**, 277 (1999)
53. N.A. Gehrels: 'Swift Gamma-Ray Burst MIDEX'. In: *X-Ray and Gamma-Ray Instrumentation for Astronomy XI*, ed. K.A. Flanagan, O.H.W. Siegmund (SPIE 4140, 2000) p.42
54. G. Gemire, L. Piro, G. Stratta, M. Garcia, J. Nichols: *GCN 782* (2000)
55. T. Giblin, J. Van Paradijs, C. Kouveliotou, V. Connaughton, R.A.M.J. Wijers, M.S. Briggs, R.D. Preece, G.J. Fishman: *Astrophys J. Lett.* **524**, L41 (1999)
56. J. Gorosabel et al.: *Astron. Astrophys. Suppl. Ser.* **138**, 455 (1999)
57. J. Greiner: *IAUC6742* (1997)
58. P.T. Groot, T.J. Galama, K. Hurley, C. Kouveliotou: *IAUC6723* (1997)
59. D. Guetta, M. Spada, E. Waxman: *Astrophys J.* **557**, 399 (2001)
60. C. Guidorzi et al.: *Astron Astrophys.* **401**, 491 (2003)
61. J. Hakkila, C.A. Meegan, G.N. Pendleton, G.J. Fishman, R.B. Wilson, W.S. Paciesas, M.N. Brock, J.M. Horack: *Astrophys J.* **422**, 659 (1994)
62. J.P. Halpern et al.: *Astrophys. J.* **543**, 697 (2000)
63. F.A. Harrison et al.: *Astrophys J. Lett.* **523**, L121 (1999)
64. F.A. Harrison et al.: *Astrophys J.* **559**, 123 (2001)
65. F.A. Harrison, A.A. Yost, S.R. Kulkarni: *GCN 1023* (2001)
66. F.A. Harrison, S. Yost, D. Fox, J. Heise, S.R. Kulkarni, P.A. Price, E. Berger: *GCN 1143* (2001)
67. J. Heise et al.: *IAUC7099* (1999)
68. J. Heise, J. in 't Zand, R.M. Kippen, P.M. Woods: in *Gamma Ray Bursts in the Afterglow Era, Proc. International Workshop at Rome, Italy, 17-20 October 2000*, eds. E. Costa, F. Frontera, J. Hjorth (Springer, Heidelberg 2001) p. 16
69. J. Heise et al.: private information (2002)
70. J. Hjorth et al.: *Astrophys J.* **576**, 113 (2002)
71. S. Holland et al.: *GCN 778* (2000)
72. K. Hurley, S. Barthelmy: *GCN 290* (1999)
73. K. Hurley et al.: *Astrophys. J.* **567**, 447 (2002)
74. G.L. Israel et al.: *Astron. Astrophys.* **348**, L51 (1999)



75. K. Iwamoto et al.: *Nature* **395**, 672 (1998)
76. R. Jager et al.: *Astron. Astrophys. Suppl. Ser.* **125**, 557 (1997)
77. R.W. Klebesadel, I.B. Strong, R.A. Olson: *Astrophys J. Lett.* **182**, L85 (1973)
78. S. Kobayashi, T. Piran, R. Sari: *Astrophys J.* **490**, 92 (1997)
79. S.R. Kulkarni et al.: *Nature* **395**, 663 (1998)
80. P. Kumar, A. Panaitescu: *Astrophys J. Lett.* **541**, L9 (2000)
81. E. Kuulkers et al.: *Astrophys J.* **538**, 638 (2000)
82. E. Kuulkers et al.: *GCN 700* (2000)
83. D.Q. Lamb: *Pub. Astron. Soc. Pacific* **107**, 1152 (1995)
84. D. Lazzati, G. Ghisellini, L. Amati, F. Frontera, M. Vietri, L. Stella: *Astrophys J.* **556**, 471 (2001)
85. D. Lazzati, E. Ramirez-Ruiz, G. Ghisellini: *Astron. Astrophys.* **379**, L39 (2001)
86. E. Le Floc'h et al.: *Astrophys J.* **581**, L81 (2002)
87. M. Livio, E. Waxman: *Astrophys J.* **538**, 187 (2000)
88. G. Manzo, S. Giarrusso, A. Santangelo, F. Ciralli, G. Fazio, S. Piraino, A. Segreto: *Astron. Astrophys. Suppl. Ser.* **122**, 341 (1997)
89. R. Manzo et al.: *GCN 956* (2001)
90. F.E. Marshall, T. Takeshima, S.D. Barthelmy, C.R.J. Robinson, K. Hurley: *IAUC6683* (1997)
91. F.E. Marshall, J.K. Cannizzo, R.H.D. Corbet: *IAUC6727* (1997)
92. F.E. Marshall, T. Takeshima, P. Woods: *GCN 138* (1998)
93. F.E. Marshall, T. Takeshima, T. Giblin, R.M. Kippen: *GCN 519* (2000)
94. N. Masetti et al.: *Astron. Astrophys. Suppl. Ser.* **138**, 453 (1999)
95. N. Masetti et al.: *Astron. Astrophys.* **374**, 382 (2001)
96. C.A. Meegan, G.J. Fishman, R.B. Wilson, J.M. Horack, M.N. Brock, W.S. Paciasas, G.N. Pendleton, C. Kouveliotou: *Nature* **355**, 143 (1992)
97. S. Mereghetti, D.I. Cremonesi, J. Borkowski: in: *Gamma-Ray Bursts in the Afterglow Era, Proc. International Workshop at Rome, Italy, 17-20 October 2000*, eds. E. Costa, F. Frontera, J. Hjorth (Springer, Heidelberg 2001) p. 363
98. P. Mészáros, M.J. Rees: *Astrophys J.* **405**, 278 (1993)
99. P. Mészáros, P. Laguna, M.J. Rees: *Astrophys J.* **415**, 181 (1993)
100. P. Mészáros, M.J. Rees, H. Papathaniassou: *Astrophys J.* **432**, 181 (1994)
101. P. Mészáros & M.J. Rees: *Astrophys J.* **476**, 2 (1997)
102. M.R. Metzger, S.G. Djorgovski, S.R. Kulkarni, C.C. Steidel, K.L. Adelberger, D.A. Frail, E. Costa, F. Frontera: *Nature* **387**, 878 (1997)
103. P. Mészáros, E. Ramirez-Ruiz, M.J. Rees: *Astrophys J.* **554**, 660 (2001)
104. P. Mészáros & M.J. Rees: *Astrophys J. Lett.* **556**, L37 (2001)
105. E. Montanari, et al. in: *Gamma-Ray Bursts in the Afterglow Era, Proc. International Workshop at Rome, Italy, 17-20 October 2000*, eds. E. Costa, F. Frontera, J. Hjorth (Springer, Heidelberg 2001) p. 195
106. T. Murakami et al.: *IAUC 6729* (1997)
107. T. Murakami, Y. Ueda, A. Yoshida, N. Kawai, F.E. Marshall, R.H.D. Corbet, T. Takeshima et al.: *IAUC 6732* (1997)
108. R. Narayan, B. Paczyński, T. Piran: *Astrophys J. Lett.* **395**, L83 (1992)
109. L. Nicastro, L. Amati et al.: *Astron. Astrophys.* **338**, L17 (1998)
110. L. Nicastro, L.A. Antonelli, G. Celidonio, M.R. Daniele, C. de Libero, G. Spoliti, L. Piro, E. Pian: *IAUC 6912* (1998)
111. L. Nicastro et al.: *Astron. Astrophys.* **138**, 437 (1999)

112. L. Nicastro, L.A. Antonelli, M. Dadina, M.R. Daniele, E. Costa, E. Pian: IAUC 7213 (1999)
113. L. Nicastro et al. in: *Gamma-Ray Bursts in the Afterglow Era, Proc. International Workshop at Rome, Italy, 17-20 October 2000*, eds. E. Costa, F. Frontera, J. Hjorth (Springer, Heidelberg 2001), p. 198
114. W.S. Paciesas et al.: *Astrophys J. Suppl.* **122**, 465 (1999)
115. B. Paczyński: *Astrophys J.* **363**, 218 (1990)
116. B. Paczyński: *Astrophys J. Lett.* **494**, L45 (1998)
117. A. Panaitescu, P. Mészáros: *Astrophys J.* **526**, 707 (1999)
118. A. Panaitescu & P. Kumar: *Astrophys J.* **543**, 66 (2000)
119. A. Panaitescu & P. Kumar : *Astrophys J.* **554**, 667 (2001)
120. A.N. Parmar et al.: *Astron. Astrophys. Suppl. Ser.* **122**, 309 (1997)
121. E. Pian et al.: *Astrophys J.* **536**, 778 (2000)
122. E. Pian et al.: *Astron. Astrophys.* **372**, 456 (2001)
123. E. Pian: Talk presented at the 3rd International Workshop on *Gamma-Ray Bursts in the Afterglow Era, held in Rome, 17-20 September 2002*
124. T. Piran: *Phys. Rep.* **314**, 575 (1999)
125. T. Piran: *Phys. Rep.* **333**, 529 (2000)
126. L. Piro et al.: *Astron. Astrophys.* **329**, 906 (1998)
127. L. Piro et al.: *Astron. Astrophys.* **331**, L41 (1998)
128. L. Piro et al.: *Astrophys J. Lett.* **514**, L73 (1999)
129. L. Piro et al.: IAUC 7111 (1999)
130. L. Piro et al.: GCN 409 (1999)
131. L. Piro et al.: *Science* **290**, 955 (2000)
132. L. Piro, G. Garmire et al.: *Astrophys J.* **558**, 442 (2001)
133. L. Piro et al.: GCN 1172 (2001)
134. L. Piro et al.: *Astrophys J.* **577**, 680 (2002)
135. L.Piro et al.: in preparation (2003)
136. P. Podsiadlowski, M.J. Rees, M. Ruderman: *Mon. Not. R. Astron. Soc.* **273**, 755 (1995)
137. M.J. Rees, P. Mészáros: *Mon. Not. R. Astron. Soc.* **258**, 41P (1992)
138. M.J. Rees & P. Mészáros: *Astrophys J. Lett.* **545**, L73 (2000)
139. J.N. Reeves et al.: *Nature* **416**, 512 (2002)
140. J.E. Rhoads: *Astrophys J.* **525**, 737 (1999)
141. G. Ricker et al.: GCN 1165 (2001)
142. G. Ricker, P. Ford, G. Monnelly, N. Butler, R. Vanderspek, D. Lamb: GCN 1185 (2001)
143. E. Rol et al.: *Astrophys J.* **544**, 707 (2000)
144. E. Rossi, D. Lazzati, M.J. Rees: *Mon. Not. R. Astron. Soc.* **332**, 945 (2002)
145. R.E. Rutledge, M. Sako: *Mon. Not. R. Astron. Soc.* **339**, 600 (2003)
146. M. Santos-Lleo, N. Loiseau, P. Rodriguez, B. Altieri, N. Schartel: GCN 1192 (2001)
147. R. Sari, T. Piran: *Astrophys J.* **485**, 270 (1997)
148. R. Sari, T. Piran: *Mon. Not. R. Astron. Soc.* **287**, 110 (1997)
149. R. Sari: *Astrophys J. Lett.* **489**, L37 (1997)
150. R. Sari, T. Piran, R. Narayan: *Astrophys J. Lett.* **497**, L17 (1998)
151. R. Sari, T. Piran, J.P. Halpern: *Astrophys J. Lett.* **519**, L17 (1999)
152. R. Sari, T. Piran: *Astron. Astrophys. Suppl. Ser.* **138**, 537 (1999)
153. R. Sari, A.A. Esin: *Astrophys J.* **548**, 787 (2001)

154. M. Schmidt: *Astrophys J. Lett.* **523**, L117 (1999)
155. A. Shemi, T. Piran: *Astrophys J. Lett.* **365**, L55 (1990)
156. I.S. Shklovskii, I.G. Mitrofanov: *Mon.Not.R.Astron.Soc.* **212**, 545 (1985)
157. P. Soffitta et al. in: *Gamma-Ray Bursts in the Afterglow Era, Proc. International Workshop at Rome, Italy, 17-20 October 2000*, eds. E. Costa, F. Frontera, J. Hjorth (Springer, Heidelberg 2001) p. 201
158. K.Z. Stanek, P. Garnavich, J. Kaluzny, W. Pych, I. Thompson: *Astrophys J. Lett.* **522**, L39 (1999)
159. G. Stratta et al. in: *Gamma-Ray Bursts in the Afterglow Era, Proc. International Workshop at Rome, Italy, 17-20 October 2000*, eds. E. Costa, F. Frontera, J. Hjorth (Springer, Heidelberg 2001) p. 118
160. T. Takeshima, C. Markwardt, F. Marshall, T. Giblin, R.M. Kippen: GCN 478 (1999)
161. M. Tavani et al: *Gamma-Ray Astrophysics 2001, Proc. Symposium at Baltimore, MD, USA, 4-6 April 2001 (AIP 2003)* in press.
162. G.B. Taylor, D.A. Frail, S.R. Kulkarni: GCN 1136 (2001)
163. C. Thompson, P. Madau: *Astrophys J.* **538**, 105 (2000)
164. J. Van Paradijs et al.: *Nature* **386**, 686 (1997)
165. J. Van Paradijs, C. Kouveliotou, R.A.M. Wijers : *Ann. Rev. Astron. Astrophys.* **38**, 379 (2000)
166. M. Vietri, L. Stella: *Astrophys J. Lett.* **507**, L45 (1998)
167. M. Vietri, G. Ghisellini, D. Lazzati, F. Fiorentini, L. Stella: *Astrophys J. Lett.* **550**, L43 (2001)
168. P.M. Vreeswijk et al.: *Astrophys J.* **523**, 171 (1999)
169. P. Vreeswijk et al.: GCN 496 (1999)
170. K.W. Weiler, L. Panagia, M.J. Montes : *Astrophys J.* **562**, 670 (2001)
171. K.W. Weiler, N. Panagia, M.J. Montes: in *Supernovae and Gamma-Ray Bursters*, ed. K.W. Weiler (Springer 2003) p. 367
172. J.C. Wheeler : IAUC 6697 (1997)
173. R.A.M.J. Wijers, M.J. Rees, P. Mészáros: *Mon.Not.R.Astron.Soc.* **288**, L51 (1997)
174. R.A.M.J. Wijers et al.: *Astrophys J. Lett.* **523**, L33 (1999)
175. S. Woosley: *Astrophys J.* **405**, 273 (1993)
176. A. Yoshida et al.: *Astron. Astrophys. Suppl. Ser.* **138**, 433 (1999)
177. J.J.M. in't Zand et al.: *Astrophys J. Lett.* **505**, L119 (1998)
178. J.J.M. in't Zand et al.: *Astrophys J.* **545**, 266 (2000)
179. J.J.M. in't Zand et al.: *Astrophys J.* **559**, 710 (2001)
180. B. Zhang, P. Mészáros: *Astrophys. J.* **559**, 110 (2001)